$KTaO_3$ Wafers Doped with Sr or La Cations for Modeling Water-Splitting Photocatalysts: 3D Atom Imaging around Doping Cations

Sasahara, Akira ; Kimura, Koji ; Hanggara, Sudrajat ; Happo, Naohisa ; Hayashi, Kouichi ; Onishi, Hiroshi

(Citation)
The Journal of Physical Chemistry C,126(46):19745-19755

(Issue Date)
2022-11-09

(Resource Type)
journal article

(Version)
Accepted Manuscript

$KTaO_3$ wafers doped with Sr or La cations for modeling water-splitting photocatalysts: 3D atom imaging around doping cations

Akira Sasahara[1], Koji Kimura[2], Hanggara Sudrajat[1,3], Naohisa Happo[4], Kouichi Hayashi[2,5], Hiroshi Onishi[1,6]*

[1]Department of Chemistry, School of Science, Kobe University, Rokko-dai, Nada, Kobe, 657-8501 Japan

[2]Department of Physical Science and Engineering, Nagoya Institute of Technology, Gokiso, Showa, Nagoya, 466-8555 Japan

[3]Research Center for Quantum Physics, The National Research and Innovation Agency, Kawasan Puspitek, Tangerang Selatan 15314 Indonesia

[4]Graduate School of Information Sciences, Hiroshima City University, Hiroshima, 731-3194 Japan

[5]Japan Synchrotron Radiation Research Institute, SPring-8, Kouto, Sayo, 679-5198 Japan

[6]Division of Advanced Molecular Science, Institute for Molecular Science, Okazaki, 444-8585 Japan

ABSTRACT. Potassium tantalate, $KTaO_3$, is a highly efficient semiconductor photocatalyst for the overall water-splitting reaction. Doping a semiconductor photocatalyst with foreign metal cations typically increases the apparent quantum yield of the splitting reaction. In this study, we constructed a single-crystalline model of cation-doped photocatalysts, which would be suitable for future investigation with advanced surface-sensitive methods. Centimeter-sized (001)-oriented $KTaO_3$ wafers were doped with Sr or La cations in KCl flux. X-ray diffraction revealed Sr- and La-containing perovskite-structured layers epitaxially covering bulk $KTaO_3$. On the Sr-doped wafer, the surface layer lattice was expanded by 2% relative to the bulk lattice. X-ray fluorescence holography was employed to determine the three-dimensional short-range ordered structure around the K and Sr cations. Holograms obtained with Sr Kα fluorescence confirmed the simultaneous settling of Sr cations in the A and B sites. The placement of the Sr cations in B sites was supported by the TaO_6 breathing vibration observed in Raman scattering. These experimental results suggested that a $KTaO_3$–$Sr(Sr_{1/3}Ta_{2/3})O_3$ solid solution is generated by doping. Two La-containing phases, one with lattice contraction by 2% and the other with expansion by 0.4%, were recognized on the La-doped wafer. La Lα fluorescence holograms indicated a complex manner of doping. The obtained atom distribution around La cations was interpreted by the simultaneous La-cation occupation at the A site, B site, and an interstitial site. Local lattice deformation was quantitatively deduced around the La cations occupying the interstitial site. Element composition determined by X-ray photoelectron spectroscopy revealed the enrichment of doping elements on the wafer surface. Nanometer-scale topography observed by atomic force microscopy suggested that doping concentrations should be optimized to provide flat, crystalline surfaces.

TOC Graphic

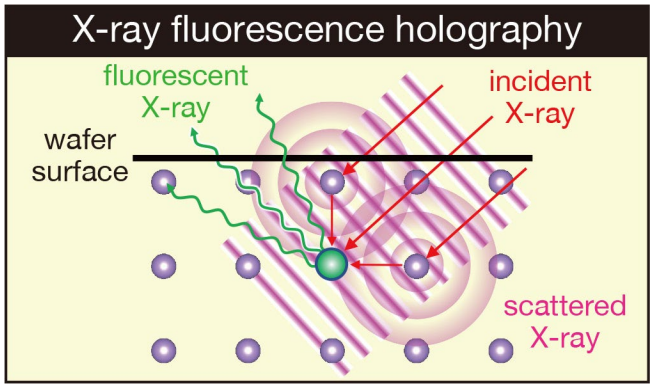

1. INTRODUCTION

Overall water splitting has been extensively investigated as a fundamental reaction for artificial photosynthesis on semiconductor photocatalysts.[1,2] Doping semiconductor photocatalysts with foreign metal cations often, but not always, increases the apparent quantum yield of the splitting reaction, which is defined as the number ratio of electrons (or holes) consumed in the reaction over the number of photons incident into the reaction vessel. In 2000, Kudo and coworkers[3] have reported that a perovskite-structured metal oxide, $NaTaO_3$, doped with La cations exhibits >50% yield, affording H_2–O_2 mixed bubbles. Doping $NaTaO_3$[4] and $KTaO_3$[5] photocatalysts with Sr cations has been reported to comparably improve its water-splitting yield. Sakata and coworkers[6] have developed Zn-doped Ga_2O_3 photocatalysts and reported an even higher yield of 70%. Recently, Takata et al.[7] have obtained a yield of almost unity on Al-doped $SrTiO_3$. However, the reason for the improvement of the quantum yield of the reaction by guest metal cations has not been revealed. In textbooks on semiconductor physics, guest metal cations are added as impurities to make the host lattice less perfect; hence, these metal cations are thought to immobilize or even recombine photoexcited electrons and holes. For

this reason, knowledge about the atom-scale structure around doping cations should be updated to reveal the aforementioned improvement.

In this study, a single-crystalline model of cation-doped photocatalysts was constructed and characterized. Centimeter-sized (001)-oriented $KTaO_3$ wafers were doped with Sr or La cations. In particular, the placement of the guest cations in the perovskite-structured $KTaO_3$ lattice was investigated. The local structure around the guest cations was determined by X-ray fluorescence holography (XFH) according to our previous studies.[8,9] XFH is a bulk-sensitive, model-free method for determining the short-range ordered 3D structure around a specific fluorescing element,[10] such as K, Sr, or La in this study.

Potassium tantalate, $KTaO_3$, exhibits a perovskite structure with a cubic symmetry and a unit cell length of 0.399 nm,[11] as shown in Figure 1. A potassium cation is located at the center of the unit cell, and it is coordinated by 12 oxygen anions. TaO_6 octahedra occupy the unit cell corners. Doping $KTaO_3$ particles with Sr,[5] La,[12,13] Hf,[14] Zr,[14] Ti,[14] Si,[14] Ga,[14] In,[14] Zn,[14] Er,[15] and Nb[16] cations is known to increase the reaction yield in photocatalytic water splitting. Single-crystal wafers of this compound have been applied for the electrochemical[17,18] and photoelectrochemical[19] oxidation of water.

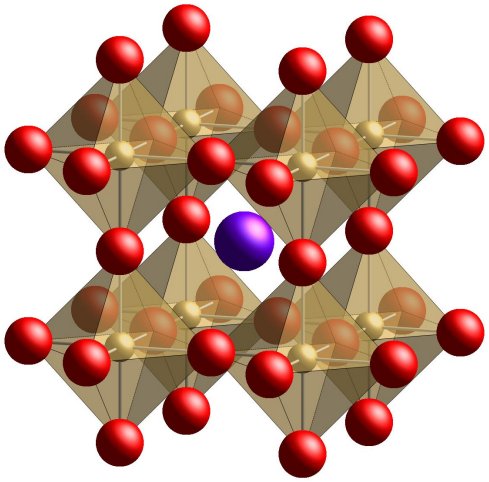

Figure 1. Ball-and-stick model of $KTaO_3$. Purple, gold, and red spheres represent potassium, tantalum, and oxygen ions, respectively.

2. METHODS

Mirror-polished $KTaO_3$(001) wafers with dimensions of 10 × 10 × 0.5 mm^3 (Crystal base) were doped with Sr or La cations in KCl flux. $SrCl_2$ (Wako) or $LaCl_3 \cdot 7H_2O$ (Wako) was mixed with KCl (99.5%, Nacalai tesque) in a molar ratio of 1:5. A $KTaO_3$ wafer was degreased in acetone, placed in an alumina crucible (15 ml) with the mixture, and heated for 48 h at 1193 K for doping with Sr or 1173 K for doping with La. The crucible was cooled to room temperature in the furnace, and solidified flux was removed with hot water. The wafer was ultrasonically washed in a HCl aqueous solution (1 mol l^{-1}) to remove Sr- or La-containing residue left on the surface, if any.

3. RESULTS

3.1. Bulk composition. The K/Ta/Sr/La atom number ratio was evaluated to be 51:49:0:0 in an as-received wafer, 77:12:11:0 in the Sr-doped wafer, and 64:28:0:8 in the La-doped wafer,

from the detection of K Kα, Ta Lα, Sr Kα, and La Lα fluorescent X-rays using a laboratory-scale spectrometer (EDX-720, Shimadzu). Doping with Sr or La cations reduced the concentration of Ta cations rather than that of K cations. However, the simple substitution of Ta cations cannot be confirmed because the escape depth of the fluorescent X-ray emissions is not the same. The depth profile of the doping elements was not known.

3.2. Crystallographic phase. X-ray diffraction (XRD) patterns were recorded using Cu Kα emission using a SmartLab (Rigaku) system in Hyogo Prefectural Institute of Technology. Figure 2 shows XRD patterns of $KTaO_3$ wafers with and without doping. Inset shows the definition of angles (θ, χ, and φ). In the XRD pattern (a) of the as-received wafer, three diffraction peaks were observed at $2\theta = 22.3°$, 45.4°, and 70.8° with $\chi = 0°$, corresponding to (00n) diffractions of $KTaO_3$ with n = 1, 2, and 3, respectively. The presence of the (00n) peaks together with the absence of other diffractions indicated that the (001) planes are stacked parallel to the wafer surface with a plane distance of 0.399 nm.

By doping with Sr cations, the (00n) diffraction was split to form satellite peaks on the low-2θ angle side, while the major peaks were still observed at the original angles, as shown in the XRD pattern (b). The satellite peaks were observed at 21.8°, 44.3°, and 68.9° (denoted by asterisks), which reveal a periodic plane distance of 0.408 nm, which was expanded by 2% relative to the distance in pristine $KTaO_3$. A portion of the wafer, probably the surface layer of a thickness less than the penetration depth of the Cu Kα X-ray, was affected by doping; hence, the lattice constant increased. The bulk volume remained intact beneath the affected layer. By doping with Sr^{2+} (9 mol%), 100 nm sized $KTaO_3$ particles[5] exhibited a low-angle shift of the (001) diffraction by 0.1° being consistent to the satellite peaks found here. The XRD pattern of

the doped wafer also revealed weak diffraction peaks at 20.3°, 25.1°, and 41.4°. Diffraction at these angles was not attributable to a perovskite structure, indicative of a limited amount of impurity phases in the probed volume.

The XRD pattern (c) shows the (00*n*) peaks of the wafer doped with La cations. Satellite peaks were observed on the high-2θ angle side of the major peaks, which was denoted by daggers. Satellite peaks were visible at 22.7°, 46.3°, and 71.8°, revealing a plane distance of 0.392 nm, i.e., 2% contraction of the lattice constant, for the surface layer affected by La doping. Liu et al.[12] prepared $KTaO_3$ particles doped with La cations (10 mol%) by a hydrothermal method and reported a high-angle shift of the (110) diffraction peak by 0.1°. The shift by 0.1° revealed a lattice contraction of 0.3%, which was less by one order of magnitude than observed in this study. A number of weak diffraction peaks were also observed at 15.6°, 19.8°, 29.0°, 31.8°, 40.3°, 49.2°, and 63.1°, suggesting a large number of impurities than those on the Sr-doped wafer.

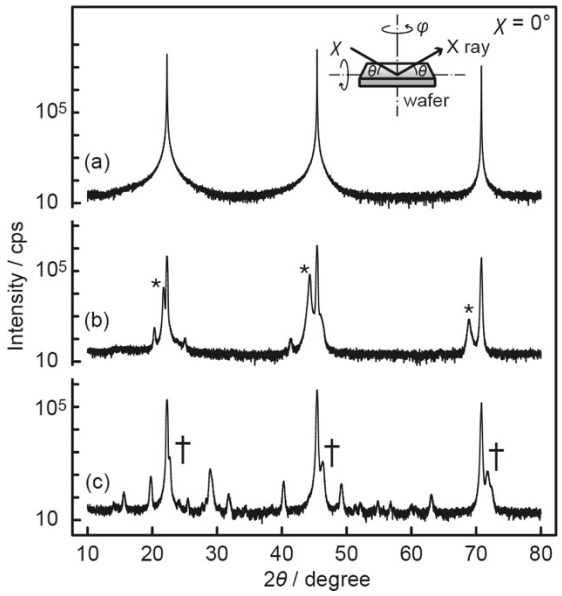

Figure 2. X-ray diffraction patterns of (001)-oriented $KTaO_3$ wafers doped with Sr or La cation. 2θ scans at $\chi = 0°$ on the (a) as-received wafers, (b) wafers doped with Sr cations, and (c) wafers doped with La cations. Diffraction intensity determined with 2θ steps of 0.01° is shown on a logarithmic scale. Inset shows the definition of angles. The satellite peaks corresponding to a plane distance affected by Sr (La) doping are denoted by asterisks (daggers).

The epitaxial relation of the $KTaO_3$ phases, one pristine phase and the other doped phase, was examined and confirmed by observing the diffraction with $\chi = 45°$ (Figure 3). In the XRD pattern (a) of the as-received wafer, one sharp peak was observed at $2\theta = 66.18°$ with $\varphi = 0°$, corresponding to the (022) diffraction for pristine $KTaO_3$. The wafers doped with Sr and La cations exhibited major peaks at identical 2θ angles (66.3° for Sr doping and 66.2° for La doping) in XRD patterns (b) and (c). A satellite peak was observed at $2\theta = 64.5°$ for the Sr-doped wafer and at $2\theta = 67.4°$ for the La-doped wafer. According to the 2θ angle of the satellites, the (011) plane distances were estimated to be 0.289 nm (Sr doping) and 0.278 nm (La doping), which are consistent with the (001) plane distances determined on the (00*n*) diffractions.

In the XRD pattern of the La-doped wafer, one additional satellite peak was observed at $2\theta = 65.9°$ on the low-angle side of the major peak (denoted by a double dagger). A shift of −0.3° relative to the major peak suggested lattice expansion by 0.4%. As this peak was not evident in the diffraction pattern with $\chi = 0°$ (Figure 2(c)), the lattice-expanded layer was thin on the top of the wafer surface. Sudrajat et al.[13] have prepared 500 nm sized $KTaO_3$ particles doped with La cations by a solid-state method. They observed a low-angle shift of the (200) diffraction peak in doped particles (10 mol%) to confirm lattice expansion by 0.2%. The lattice-expanded layer,

which caused the double-daggered peak on our wafer, was possibly a phase common to that Sudrajat et al. found in particles. On the other hand, Sudrajat et al.[13] did not recognize the lattice-contracted phase that was evident on our wafer. The presence and absence of the lattice-contracted phase are supposedly related to the different environments during La doping. A large excess of K cations was available in KCl flux to fill A sites in $KTaO_3$, while it was not available by the solid-state method.

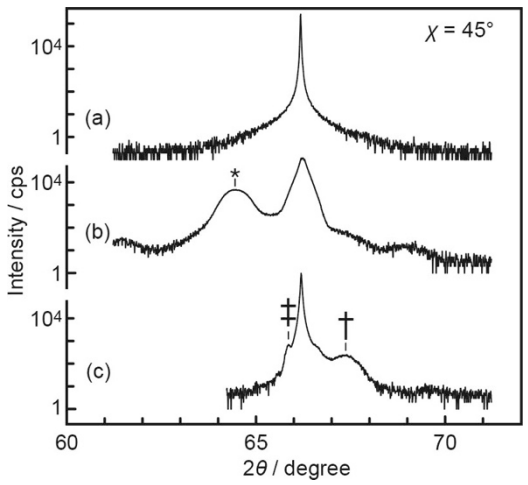

Figure 3. X-ray diffraction patterns of the $KTaO_3$ wafers. 2θ scans at $\chi = 45°$ and $\varphi = 0°$ of the (a) as-received wafers, (b) wafers doped with Sr cations, and (c) wafers doped with La cations. Diffraction intensity determined with 2θ steps of 0.01° is presented on a logarithmic scale. The satellite peak affected by Sr (La) doping is denoted by an asterisk (dagger). An additional peak is detected on the low-angle side of the La-doped wafer (double dagger).

φ was further scanned from −45 to +315° with $\chi = 45°$. In the φ scans shown in the left panels of Figure 4, the diffraction at $2\theta = 66.2°$ exhibited four peaks at $\varphi = 0°$, 90°, 180°, and 270° for the doped wafers, according to the fourfold symmetry of bulk $KTaO_3$. Another φ scan with $2\theta = 64.5°$ (Sr-doped wafer) or 67.4° (La-doped wafer) exhibited an identical fourfold

pattern, confirming the epitaxial relation of the doped layers on the pristine bulk volume. In-plane alignment of the doped layers and pristine volume was inspected by the intensity plots around $\varphi = 0°$ in the right panels. The surface and bulk phases exhibited one maximum centered at 0° with no sign of a rotational misfit across the phase boundary. This result was in contrast to the reported observation of $KTaO_3$ wafers doped with Ca cations,[9] where Ca-containing surface domains were rotated by ±1.0° on the bulk lattice. The different rotational alignments may have been induced by different size of doping cations or different doping methods; Sr and La cations were doped in KCl flux in this study, while Ca cations were doped without the flux in ref. 9.

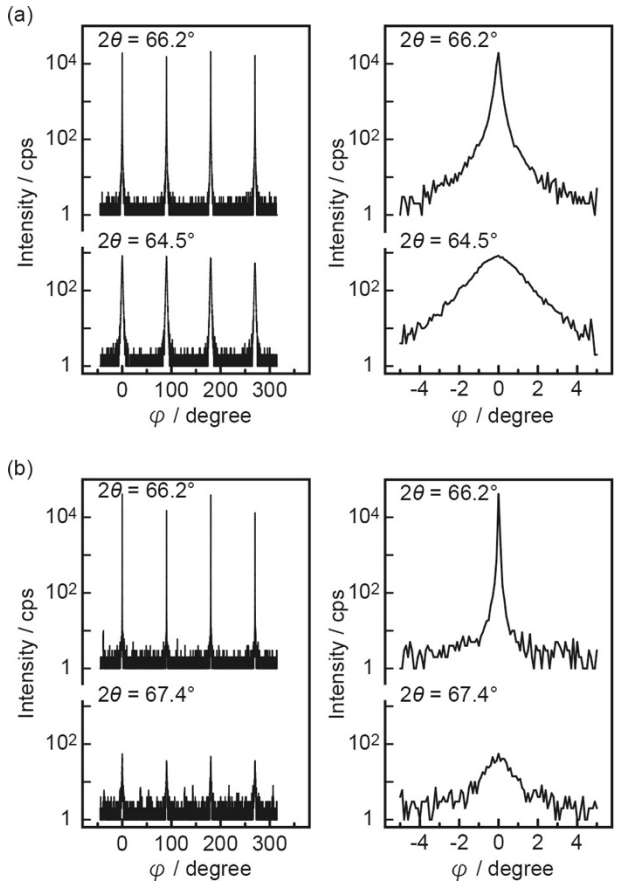

Figure 4. X-ray diffraction patterns of the $KTaO_3$ wafers. φ scans at $\chi = 45°$ on the wafers doped with (a) Sr and (b) La cations. Diffraction intensity determined with φ steps of 0.1° is presented on a logarithmic scale.

3.3. Local structure around K, Sr and La cations. The long-range ordered structure of the doped wafers was characterized by XRD to reveal lattice expansion by 2% with Sr doping, as well as contraction by 2% and expansion by 0.4% with La doping. In this subsection, the local structure around the guest cations was evaluated by XFH.

A wafer of interest was irradiated with a plane-wave X-ray (Figure 5). Atoms B and C that were adjacent to atom A scattered the incident X-ray. The scattered wave superimposed on the incident wave created a standing wave, producing a fluorescent X-ray of atom A. Fluorescence intensity is proportional to the standing-wave intensity on atom A; hence, it is sensitive to the angles of X-ray incidence, θ and ϕ.

In this study, K Kα, Sr Kα, and La Lα emissions were observed in the beamline 13XU of the SPring-8 facility. Curved graphite crystals[20] were used to focus the fluorescent X-ray on a point detector. The $KTaO_3$ wafer of interest was set on a goniometer, and fluorescence intensity $I(\theta)$ was observed in a θ range of 0°–75° in 1° steps at one azimuth angle, ϕ. Similar θ scans were repeated at different ϕ values of 0°–360° in steps of 0.25° to complete one hologram, $I(\theta, \phi)$. By applying Barton's algorithm[21] to a set of holograms that were determined with an incident X-ray of different wavelengths, the 3D distribution of X-ray scattering atoms was reconstructed around the fluorescing atom A. The 3D-AIR-IMAGE code[22] was used for reconstruction.

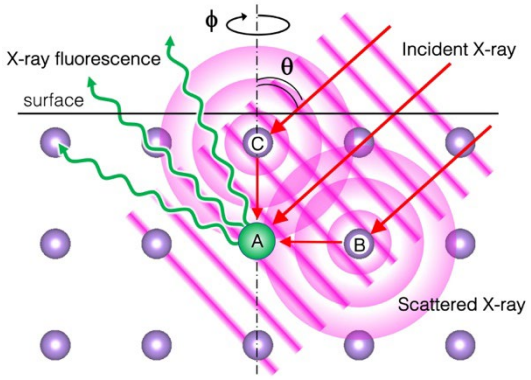

Figure 5. Principle of X-ray fluorescence holography.

3.3.1. Structure around potassium cations. One of the host elements, K, was examined as the cation that selectively occupied the A site in the perovskite-structured $KTaO_3$ lattice. Six holograms were acquired on the La-doped wafer by detecting potassium Kα emission under excitation with X-rays at 7.50, 8.00, 8.50, 9.00, 9.50, and 9.75 keV. The holographic oscillation $\chi(\theta, \phi)$ was obtained with raw $I(\theta, \phi)$ as

$$\chi(\theta,\phi) = \frac{I(\theta,\phi) - I_0(\theta,\phi)}{I_0(\theta,\phi)}$$

with the background intensity $I_0(\theta, \phi)$.[23] A three-dimensional distribution of X-ray scattering atoms, atomic image, was reconstructed in a cubic volume of $(2\ \text{nm})^3$ centered at the fluorescing K cation, where *x*-, *y*-, and *z*-axes were respectively parallel to the [100], [010], and [001] directions of the $KTaO_3$ lattice.

The upper panel of Figure 6(a) shows the atomic images on an *xy* plane at $z = 0$ sliced from the reconstructed volume. Substantial scattering spots were not recognized around the fluorescing K cation placed at (0, 0, 0). Weak spots were ascribed to the artifacts produced during the numerical process of reconstruction. Oxygen anions are present at (0.20 nm, 0.20 nm) and at equivalent positions in accordance with the fourfold symmetry, as illustrated in the lower

panel. However, they were missing in the atomic images in the upper panel. Missing oxygen anions were observed in the reconstruction on lanthanum Lγ holograms of $SrTiO_3$ doped with La cations,[24] niobium Kα holograms of $Pb(Fe_{1/2}Nb_{1/2})O_3$,[25] as well as calcium Kα and barium Lγ holograms of $(Ba_{0.9}Ca_{0.1})TiO_3$.[26] The missing anions are interpreted with the limited X-ray scattering power of oxygen relative to that of tantalum.

Potassium cations in $KTaO_3$ also should be present on the plane, but they were invisible. The first-nearest K cations are located at (0.40 nm, 0.00 nm) and equivalent positions. The missing cations are related to the limited X-ray-scattering power of potassium. Tantalum cations are absent on this plane according to the crystallographic structure of $KTaO_3$.

On the *xy* plane of z = 0.20 nm, four first-nearest Ta cations were observed at (0.19 nm, 0.19 nm), together with eight second-nearest Ta cations at (0.19 nm, 0.60 nm), as displayed in the upper panel of Figure 6(b). Again, oxygen anions were missing even at the first-nearest position, i.e., (0.20 nm, 0.00 nm).

On the two planes, Ta cations were recognizable, whereas O anions and K cations were missing. The assumption of dominant X-ray scattering by Ta cations in $KTaO_3$ was verified. The authors noted the selective recognition of Ta cations in $KTaO_3$ with Ta Lα holograms where X-ray scatterers were reconstructed around the fluorescing Ta cation (Figure 5 of ref. 9). The Sr and La holograms observed herein were interpreted on this assumption in the following sections.

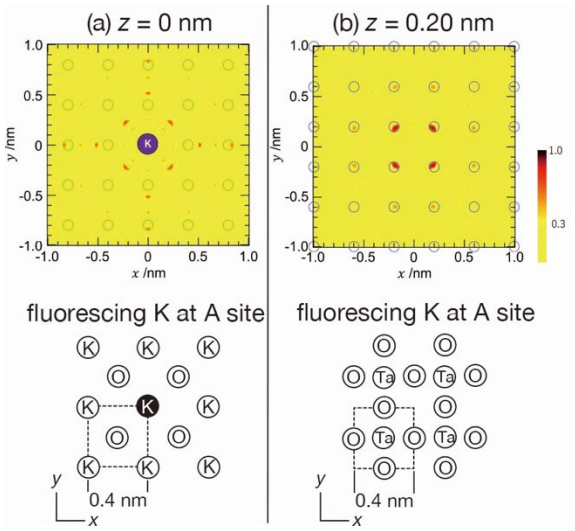

Figure 6. Atomic images reconstructed from potassium Kα holograms on the La-doped $KTaO_3$ wafer. (a) 2D distribution of X-ray scattering objects on a plane of $z = 0$ is shown in the upper panel. The scale bar shows scattering intensity normalized to 0–1. The fluorescing potassium cation is located at (0, 0, 0), which is labeled as "K." Circles indicate the K-cation sublattice in $KTaO_3$. The placement of eight potassium and four oxygen ions on the plane is depicted in the lower panel with a 2D unit cell of the perovskite-structured lattice (broken line). (b) Atom distribution on a plane of $z = 0.20$ nm is shown in the upper panel. Circles indicate the Ta cation sublattice in $KTaO_3$. The placement of 4 tantalum and 12 oxygen ions on the plane is depicted in the lower panel.

3.3.2. Structure around strontium cations. Eight Sr Kα holograms were obtained on the Sr-doped wafer with incident X-ray of 17.0–20.5 keV with 0.5 keV steps. On the *xy* plane of $z = 0$ (Figure 7(a)), atomic images were observed periodically on a square lattice with side lengths of 0.40 nm. First-, second-, third-, fourth-, and even fifth-nearest atoms were visible, revealing a well-ordered structure around the fluorescing Sr cation. The square lattice of reconstructed atoms was ascribed to the Ta cation sublattice on the assumption verified in section 3.3.1. The

fluorescing cation located at (0, 0, 0) was precisely incorporated in the sublattice. Hence, the fluorescing Sr cation occupies the B site in exchange for a Ta cation.

On the *xy* plane of $z = 0.20$ nm shown in panel (b), we observed four first-nearest Ta cations at (0.19 nm, 0.19 nm) and equivalent positions, while second-nearest cations were missing, and we observed the third-nearest ones at (0.58 nm, 0.58 nm). The Ta cations were placed in a manner identical to those reconstructed with K Kα holograms on the plane of $z = 0.2$ nm (Figure 6(b)). The identical placement suggested that the fluorescing cation exhibits an identical position in the host lattice; the fluorescing Sr cation occupies A sites in exchange for a K cation. The Ta cation distribution on the plane of $z = 0$ confirmed Sr cations at the B site, as described in the preceding paragraph, whereas the distribution on the plane of $z = 0.20$ nm confirmed the settling of Sr cations in the A site. The two statements can be acceptable only when Ta and K cations were simultaneously doped with Sr cations.

The simultaneous occupation of the A and B sites concluded here was fully consistent to an extended X-ray absorption fine structure (EXAFS) study of Sr-doped $KTaO_3$ particles.[5] Double substitution for Ta and K cations was suggested on the basis of two Sr–O lengths, 0.24 and 0.27 nm, recognized in EXAFS. The short Sr–O length was ascribed to SrO_6 octahedra with the Sr cations occupying B site. The long length was assigned to SrO_{12} cuboctahedra with the cations settling in A site. In $NaTaO_3$ particles[27] and films[28] doped with Sr cations, EXAFS of Sr K edge was analyzed to show two Sr–O lengths in line with the observation on Sr-doped $KTaO_3$ particles.[5]

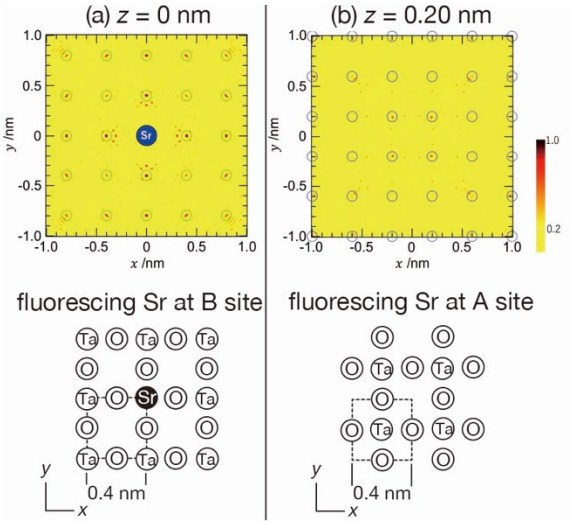

Figure 7. Atomic images reconstructed from Sr Kα holograms on the Sr-doped $KTaO_3$ wafer. (a) 2D distribution on a plane of $z = 0$ is shown in the upper panel. The fluorescing Sr cation located at (0, 0, 0) is labeled as "Sr." Circles indicate the Ta cation sublattice when the fluorescing cation settled in the B site. The placement of 8 Ta and 12 oxygen ions around the fluorescing cation at the B site is depicted in the lower panel with a 2D unit cell (broken line). (b) Distribution on a plane of $z = 0.2$ nm is shown in the upper panel. Circles indicate the Ta cation sublattice when the fluorescing Sr cation settled in the A site. The placement of 4 tantalum and 12 oxygen ions on the plane is depicted in the lower panel.

3.3.3. Structure around lanthanum cations. Figure 8 shows the atomic images around a fluorescing La cation, which were reconstructed with nine La Lα holograms on the La-doped wafer (incident X-ray energy: 7.5–11.5 keV with 0.5 keV steps). The atomic images were more complicated than those reconstructed around the K or Sr cation. The authors hypothesized the simultaneous occupation of the La cation at the A site, B site, and an interstitial site to interpret the observed images. Figure 8(a) shows the three hypothesized sites: La(A), La(B), and La(I).

On the *xy* plane of $z = 0$, four Ta cations were observed at (0.40 nm, 0.00 nm) and equivalent positions, as shown in the top panel of (b). The fluorescing La cation located at (0, 0, 0) was incorporated in the square lattice of the four Ta cations, indicative of its settling in the B site as depicted in the middle panel. The second-nearest or beyond tantalum cations were missing, suggesting a less-ordered structure around La(B) than that around the Sr cation at the B site (Figure 7(a)).

In addition to the Ta cation at (0.40 nm, 0.00 nm), two more atoms were observed on the *xy* plane of $z = 0$: one at (0.24 nm, 0.24 nm) and the other at (0.68 nm, 0.17 nm). The additional atoms were present approximately on a square lattice marked with red circles, but these atoms were distorted to form a trapezoidal placement, as outlined by solid lines. The square lattice of red circles was fitted to the Ta cation sublattice neither around an A-site cation nor around a B-site cation. We hypothesized that the fluorescing cation occupied an interstitial site, La(I), to interpret the additional atom images. The bottom panel of Figure 8(b) shows the atom placement expected around La(I). The first- and second-nearest Ta cations around La(I) reproduced the red-circled atoms. The trapezoidal distortion was natural to make room for accommodating an additional La cation in the interstitial position. The first-nearest Ta cations were displaced at 0.06 nm away from their original positions to induce the trapezoidal distortion.

Figure 8(c) shows the atom distribution on the *xy* plane of $z = 0.20$ nm. Four Ta cations were observed at (0.21 nm, 0.21 nm) and equivalent positions. The observed Ta cation placement was identical to that on the same plane reconstructed by potassium Kα holograms (Figure 6(b)) although second-nearest cations were missing. Fluorescing cations settled in the A sites, La(A), were required to interpret the Ta cation placement in this manner.

According to EXAFS reported by Sudrajat et al.[13], the La–O length in La-doped $KTaO_3$ particles was 0.25–0.26 nm. This length fitted La(A) as the K–O length was 0.28 nm in pristine $KTaO_3$. On the other hand, the reported La–O length was long for La(B) and La(I). In La-doped $NaTaO_3$ particles,[29] EXAFS of La K edge showed one La–O length, 0.25 nm. When La cations occupied three different sites as hypothesized in the present study, a number of slightly different La–O lengths were possibly recognized as one La–O length in curve fitting analysis.

Another La K edge study[30] reported complicated radial distribution in the first coordination shell in La-doped $NaTaO_3$ particles. These earlier EXAFS studies suggested one-dimensional radial distribution is not enough to determine complicated local structure around La cations embedded in $KTaO_3$ and $NaTaO_3$ matrices. The authors thus conducted atom mapping with XFH in the present study to reveal 3D structure around La cations in $KTaO_3$.

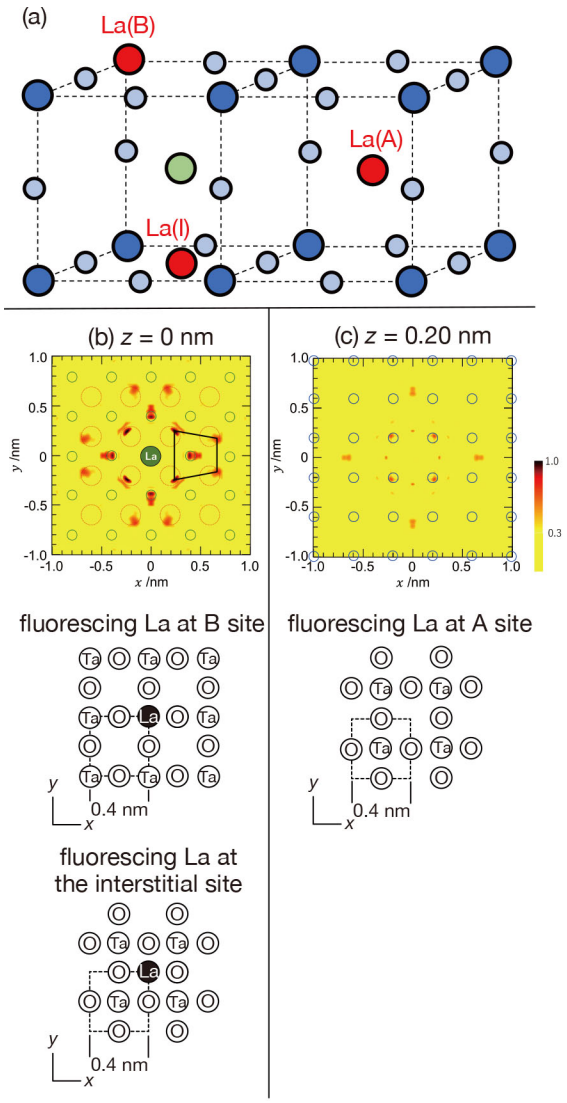

Figure 8. Atomic images reconstructed from La Lα holograms on the La-doped $KTaO_3$ wafer. (a) 3D description of hypothesized placements of the La cation, La(A) at the A site, La(B) at the B site, and La(I) at an interstitial site. (b) Atomic images reconstructed on an *xy* plane of *z* = 0. The fluorescing La cation is located at (0, 0, 0), which is labeled as "La." Small green circles indicate the Ta cation sublattice around La(B). Large red circles represent the Ta cation sublattice around La(I). The Ta cation sublattice distorted around La(I) is outlined by solid lines. The placement of 8 Ta and 12 oxygen ions is depicted around La(B) in the middle panel. The bottom panel shows the Ta cation sublattice when the fluorescing cation occupies La(I). (c)

Atom distribution on an *xy* plane of $z = 0.20$ nm. Circles indicate the Ta cation sublattice when the fluorescing La cation is settled in the A site.

3.4. Lattice vibration probed by Raman scattering. Raman scattering of the $KTaO_3$ wafers was observed with green excitation light (532 nm, 60 mW) at room temperature using an NRS-7100 spectrometer (Jasco). Figure 9(a) shows the spectrum of the as-received wafer with vibrational bands at 278, 461, 590, 696, 740, and 890 cm^{-1}. These bands corresponded to second-order Raman transitions (combination tones and overtones) as all of the first-order phonon modes were forbidden under the cubic symmetry in the $KTaO_3$ lattice.[31]

On the wafer doped with Sr cations, an intense band also was observed at 812 cm^{-1}, as shown in panel (b). The presence of this band indicated a B-site-substituted perovskite, $AB_{1-x}B'_xO_3$. The breathing vibration of BO_6 octahedra, exhibiting A_{1g} symmetry, cannot contribute to Raman scattering in a cubic perovskite ABO_3 because of the symmetry-driven selection rule. The cubic symmetry around a BO_6 octahedron adjacent to a $B'O_6$ in $AB_{1-x}B'_xO_3$ was broken to allow scattering coupled with the breathing vibration. Actually, the breathing vibration produced intense Raman bands at 780–850 cm^{-1} in $Ba(Mg_{1/3}Ta_{2/3})O_3$, $Pb(Mg_{1/3}Ta_{2/3})O_3$, $Pb(Mg_{1/2}W_{1/2})O_3$, and $Sr(Li_{1/4}Ta_{3/4})O_3$.[32,33] Hence, the band at 812 cm^{-1} in Figure 9(a) reveals Sr cations settled in B sites. On the other hand, the selection rule did not provide affirmative or negative evidence of A-site substitution. A-site-substituted perovskites, $(Na_{1/2}Bi_{1/2})TiO_3$,[32] and $NaTaO_3$ doped with K cations,[34] did not exhibit additional Raman bands.

The spectrum of the La-doped wafer exhibited a finite increase in the intensity at 800 cm^{-1}. In the case of the as-received wafer, a second-order band was observed at 740 cm^{-1}, with a downhill slope to 850 cm^{-1}. By doping with La cations, we observed an additional band at 800

cm^{-1}, and it merged with the band at 740 cm^{-1}, creating a plateau at 740–800 cm^{-1}. The La-induced band at 800 cm^{-1} was weak in comparison with that at 812 cm^{-1} induced by Sr doping. The different intensities were attributed to different concentrations of La cations settling in the B sites and/or TaO_6 octahedra locally distorted around La(I).

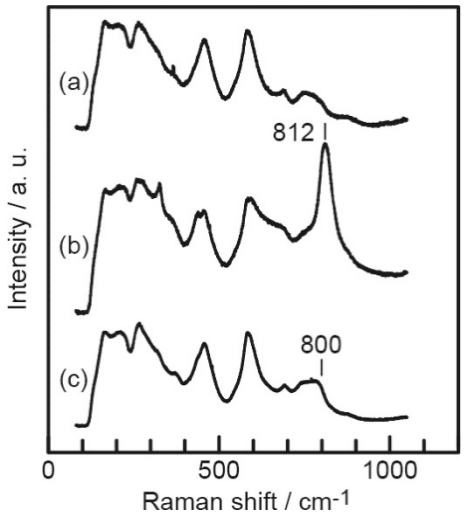

Figure 9. Raman spectra of the (a) as-received, (b) Sr-doped, and (c) La-doped $KTaO_3$(001) wafers.

3.5. Surface topography. The wafers were scanned by an atomic force microscope (SPM-9600, Shimadzu) operated in the contact mode using silicon nitride cantilevers (OMCL-TR800PSA, Olympus). Figure 10(a) shows the flat and smooth topography of the as-received wafer. A cross-section determined on the dotted line indicated a corrugation less than 4 nm in panel (d). Broad stripes parallel to the [001] direction were recognized in (a) and attributed to uneven polishing. Similar stripes were observed on other as-received wafers in different directions.

Irregularly faceted protrusions covered the Sr-doped wafer, as shown in Figure 10(b). The typical size of protrusions was 1 μm in the lateral dimension and 0.5 μm in the vertical

dimension, as shown in (d). XRD and XFH results indicated that the Sr-doped portion epitaxially crystallizes on bulk $KTaO_3$. The irregularly oriented corrugations conflicted with the epitaxial nature of doped portions. The topmost surface probed by AFM was probably covered with materials without an epitaxial relationship, and the thickness of the materials was insufficient to produce their signatures in XRD and XHF.

Figure 10(c) shows the surface of the La-doped wafer: Rectangular islands with flat facets on the top were observed. The lateral boundary of the islands was oriented to the [100] or [010] direction, unlike the irregular corrugations on the Sr-doped wafer. The oriented boundaries suggested the epitaxial relationship of the surface material on bulk $KTaO_3$, which was in accordance with the XRD and XFH results.

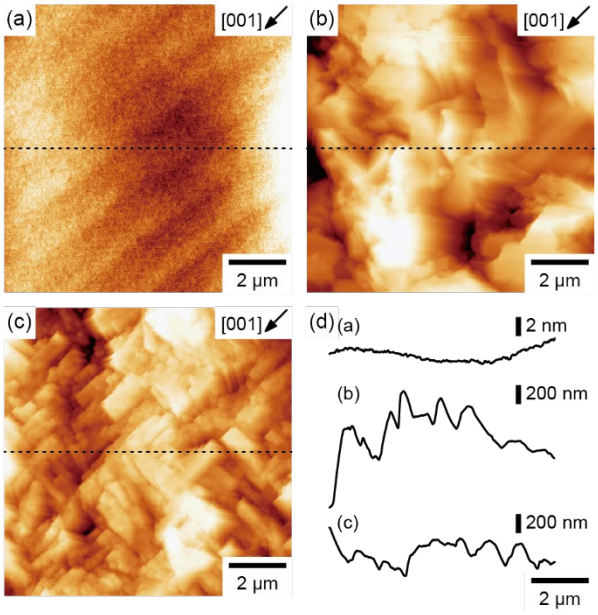

Figure 10. Contact-mode AFM images of the (a) as-received, (b) Sr-doped, and (c) La-doped $KTaO_3$(001) wafers. Image size: 10 μm × 10 μm. Cross-sections were determined along the dotted lines and depicted in (d). Raw images were presented in (a)–(c), and the cross-sections were determined on the images smoothed with a nine-point median filter.

3.6. Surface composition. X-ray photoelectron spectra (XPS) were recorded using monochromatized Al Kα emission in a spectrometer (PHI X-tool, ULVAC-PHI). Binding energy was calibrated such that the O 1s peak of bulk $KTaO_3$ was observed at 530.0 eV. Potassium, tantalum, and oxygen were detected in the survey-scan spectrum of the as-received wafer shown in Figure S1 (Supporting Information). Strontium and lanthanum were additionally recognized in survey scans of the Sr-doped and La-doped wafers. No other element was detected except carbon. Chlorine was absent although the wafers were heated in KCl flux.

Figure 11(a) shows a set of narrow-scan spectra of the as-received wafer. The O 1s emission was fitted with three peaks, namely, a major peak at 530.0 eV accompanied by two minor peaks at 530.8 and 532.3 eV. The major peak was ascribed to oxygen anions in bulk $KTaO_3$. The peak at 530.8 eV was ascribed to oxygen anions coordinated by fewer cations possibly at the surface. The peak at 532.3 eV possibly corresponded to surface-adsorbed OH species. When the $KTaO_3$(001) surface was cleaved in an ultrahigh vacuum and exposed to H_2O vapor,[35] O 1s emission was observed at a binding energy greater by 1.6 eV than that of the emission from the bulk and assigned to surface OH species. Tantalum 4f emission was characterized by the 7/2 and 5/2 splitting peaks at 26.1 and 28.0 eV corresponding to Ta^{5+}.[12,36] Potassium 2p emission was characterized by the 3/2 and 1/2 splitting peaks of K^+ cations at 291.8 and 294.6 eV, respectively.

In the case of the Sr-doped wafer, O 1s peaks at 530.8 and 532.3 eV were strengthened (Figure 11(b)). The surface was corrugated according to the AFM images. It is reasonable that population of less-coordinated oxygen anions and OH species increased on the corrugated surface. The peak width of Ta 4f emissions increased, suggesting heterogeneous environments

around surface Ta^{5+}, while the peak energy remained intact. The twin peaks at 133.7 and 135.5 eV were attributed to 5/2 and 3/2 splitting of Sr 3d emissions, respectively. The binding energy of the 5/2 peak was in agreement with that observed on $SrTiO_3(001)$.[37,38] The K 2p emission was not detected. The missing potassium signal was unexpected, and it was interpreted as Sr cations enriched on the surface. The escape depth of K 2p photoelectrons was ca. 2 nm. The irregularly corrugated topography of the doped wafer (Figure 10(b)) was in agreement with the supposed enrichment.

Figure 11(c) shows narrow-scan spectra of the La-doped wafer. The O 1s spectrum was fitted with three components. Tantalum 4f peaks did not exhibit a shift. The La 3d 5/2 state exhibited a peak at 834.5 eV, which was consistent with the binding energy of La^{3+} reported previously. The other peak at 839.2 eV reflected another final state in which electrons of oxygen anions were transferred to empty 4f orbitals of La^{3+}.[39,40] Again, the K 2p emission was absent.

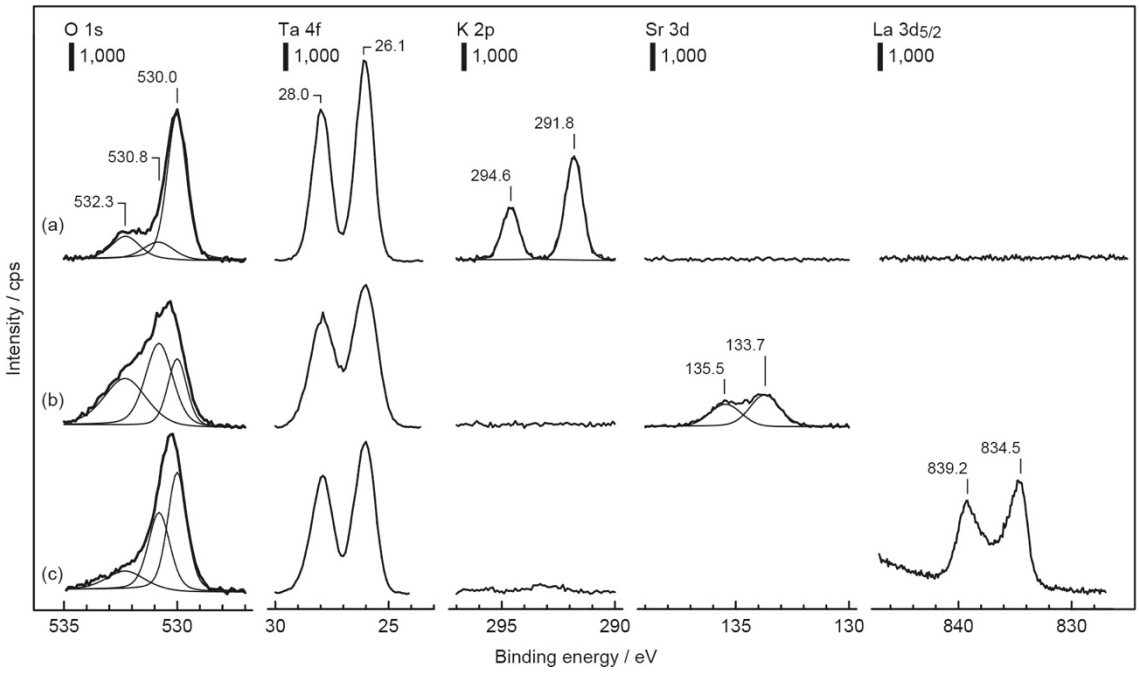

Figure 11. Narrow-scan XPS spectra of (a) as-received, (b) Sr-doped, and (c) La-doped $KTaO_3$(001) wafers. Analyzer pass energy: 26 eV.

4. DISCUSSION

4.1. Doping with Sr cations. Doping with Sr cations led to the $KTaO_3$ lattice expansion by 2% as quantified by XRD. XFH confirmed the double occupation of Sr cations at the A and B sites. The selection rule for Raman scattering indicated that the cubic symmetry around TaO_6 octahedra in the doped wafer is broken. The three findings were consistent.

The selective exchange of potassium cation would cause lattice contraction according to the ionic radii shown in Table 1. Tantalum cations were simultaneously exchanged with Sr cations to expand the lattice. Double doping to the A and B sites provided a way to balance cationic and anionic charges without creating oxygen anion vacancies. Experimental[34] and theoretical[41] studies confirmed that the doping of $NaTaO_3$ particles with Sr cations in this manner forms a $NaTaO_3$–$Sr(Sr_{1/3}Ta_{2/3})O_3$ solid solution. In $KTaO_3$ wafers examined in this study, an analogous $KTaO_3$–$Sr(Sr_{1/3}Ta_{2/3})O_3$ solid solution was probably formed.

The tolerance factor of the solid solution is considered to estimate the stability of the doped $KTaO_3$ lattice under a hard-sphere approximation. The factor is defined by $\frac{r_A+r_O}{\sqrt{2}(r_B+r_O)}$ with radii of the A-site cation (r_A), B-site cation (r_B), and oxygen anion (r_O). The lattice fulfilled by the hard-sphere ions gives a factor of unity. Hence, a cubic perovskite structure is a reasonable possibility with factors of 0.9–1.0.[42]

$KTaO_3$ exhibited a factor of 1.06 according to the radii shown in Table 1. The radius of oxygen anion was assumed to be 0.137 nm as the simple average of the two radii in the table

since an oxygen anion was coordinated simultaneously with four A-site cations and two B-site cations. A tolerance factor of 0.97 was obtained in $Sr(Sr_{1/3}Ta_{2/3})O_3$, where r_B was assumed to be 0.082 nm as a population-weighted average of the Sr and Ta radii. The Sr-rich end of the solid solution, $Sr(Sr_{1/3}Ta_{2/3})O_3$, is known as a real compound.[43,44] The solid solution of $KTaO_3$ and $Sr(Sr_{1/3}Ta_{2/3})O_3$ should exhibit a cubic perovskite structure with tolerance factors in the range of 1.06–0.97.

In a DFT study by Tang et al.,[41] doping of $NaTaO_3$ with Sr cations was examined. They reported that double doping at Na and Ta sites significantly reduces the formation energy of the Sr dopant cations compared with that predicted in single doping at Na site or Ta site (Figure 3 of ref. 41). In a thermodynamical equilibrium, which should be dominant in photocatalyst preparation at elevated temperatures, the two sites are simultaneously occupied by Sr dopant cations for energy stability.

Table 1. Ionic radii according to ref. 45. Coordination numbers are in parentheses.

Ion	Radius / nm
K^+	0.164 (12)
Ta^{5+}	0.064 (6)
Sr^{2+}	0.118 (6), 0.144 (12)
La^{3+}	0.103 (6), 0.136 (12)
O^{2-}	0.135 (2), 0.138 (4)

4.2. Doping with La cations. Local structures created by doping with La cations were far more complex than those created by doping with Sr cations. The complex structures were

reflected in two phases found in XRD and the three sites for accommodating La cations evidenced by XFH.

Atomic images reconstructed on the holograms suggested that La cations settle simultaneously in the A and B sites. The placement of La cations at the B site was supported by the Raman band at 800 cm^{-1}, which corresponds to a signature for broken symmetry. These results offer a possibility of double doping to make a solid solution as is claimed for Sr doping. However, a simple extension of the $KTaO_3$–$Sr(Sr_{1/3}Ta_{2/3})O_3$ solid solution is problematic. As La cations are selectively in the 3+ oxidation state, the solution composition should be $KTaO_3$–$LaLaO_3$ in the absence of a cation or an anion vacancy. $LaLaO_3$ is a virtual compound in which one La cation is accommodated in the A site, while the other occupies the B site in its perovskite-structured lattice. The virtual $LaLaO_3$ requires a tolerance factor of 0.80, reflecting the oversized La cation in the B site.

Another issue to be considered is the balance of cationic and anionic charges. The single exchange for the A-site cation occurred in La-doped $SrTiO_3$ where the doped materials exhibited a metallic property and a deep blue color.[46] As the settling of La(A) cations in the La-doped $KTaO_3$ wafer was confirmed by XFH, electrons should have been donated to the host material accordingly as the source of blue color. However, after doping with La cations, $KTaO_3$ wafers and particles remained transparent or white, indicative of their intact wide-bandgap property. The donated electrons could be compensated by two routes. One is La substitution for Ta^{5+} in the B-site to make a $KTaO_3$–$LaLaO_3$ solid solution despite the presence of oversized La cations in the B site. The other requires cation vacancies in the doped materials.

In addition to settling in the A and B sites, the holograms allowed us to hypothesize that some La cations occupied an interstitial site (Figure 8(a)). This hypothesis needs to be tested further because the perovskite-structured $KTaO_3$ lattice is filled by the cations and anions at ordinary sites with limited room for accommodating an additional cation at the interstitial position. Energetic stability of La cation at different sites should be revealed in the future by incorporating an electronic interpretation using DFT calculations.

Our XRD results (Figure 3(c)) revealed two La-containing phases; one with lattice contraction by 2% and the other with expansion by 0.4%. The hypothesized $KTaO_3$–$LaLaO_3$ solution was in agreement with the expanded lattice due to the oversized B-site cations. A-site doping accompanied with cation vacancy creation was favorable for the lattice-contracted phase.

4.3. depth dependence of dopant concentration. Surface X-ray diffraction indicated a Sr-containing or La-containing, crystalline $KTaO_3$ layer was present epitaxially on the pristine $KTaO_3$ substrate. The authors assume that short-range ordered structures in the epitaxial layers were recognized in XFH. The topmost surface of different composition was present on top of the epitaxial layers. Dopant segregation to the surface was reported on $NaTaO_3$[29,47] as well as $KTaO_3$[5] photocatalyst particles. The thickness of the dopant-rich layers was 3–4 nm on top of 100 nm sized particles according to element mapping of scanning transmission electron microscopy.

The doped wafers exhibited an unexpectedly small surface concentration of potassium in XPS and heavily corrugated topography in AFM. These properties are unfavorable as a platform for surface characterization. Optimizing doping concentration and doping method are necessary to remove significant segregation of dopant cations for future studies with advanced surface-

sensitive methods. Pulsed laser deposition is feasible for preparing doped films epitaxially on $KTaO_3$ or $SrTiO_3$ substrate. Actually, Sr-doped $NaTaO_3$ films (thickness: 100 nm) were deposited on $SrTiO_3$ (001) substrate.[28] However, the thickness of object films should be 1 μm or more to acquire holographic oscillation in XFH. Pulsed laser deposition of μm-thick films is not straightforward.

4.4. Reaction rate evaluation on doped wafers. It was difficult to determine photocatalytic reaction rate over single-crystalline wafers, since the surface area of the wafers was limited to be 1 cm^2. In ordinary reaction rate evaluation, photocatalyst particles (typically 0.5 g) are suspended in water and irradiated with excitation light. The specific surface area of photocatalyst particles is around 2 $m^2\ g^{-1}$. Interface area of the photocatalyst and water should be in the order of 1 m^2 in the suspension. The amount of reaction products is sensitive, often proportional, to the interface area. The authors are currently developing a microelectrode-based method feasible for reaction rate evaluation on cm-sized photocatalyst films and wafers.[48,49] Photocatalytic reaction rate is to be evaluated over doped wafers in future studies.

5. CONCLUSION

In this study, platforms were produced for surface science studies of artificial photosynthesis on cation-doped $KTaO_3$ photocatalysts. Centimeter-sized single-crystalline wafers were doped with Sr or La cations in KCl flux. X-ray diffraction revealed Sr- and La-containing perovskite-structured layers covering bulk $KTaO_3$. On the Sr-doped wafer, the surface layer lattice was expanded by 2% relative to the bulk lattice. The short-range ordered structure around the K and Sr cations was determined by X-ray fluorescence holography. We detected the first-, second-, and third-nearest Ta cations around the K cation emitting Kα fluorescence, whereas the

neighboring K cations and O anions were missing because of their limited X-ray-scattering power. Holograms obtained with Sr Kα fluorescence were analyzed by this rule to confirm the simultaneous settling of the Sr cations in the A and B sites. The placement of the Sr cations in the B sites was supported by the TaO_6 breathing vibration observed in the Raman scattering. These experimental results were completely consistent to the $KTaO_3$–$Sr(Sr_{1/3}Ta_{2/3})O_3$ solid solution proposed in earlier EXAFS studies conducted on nanometer-sized photocatalyst particles. Two La-containing phases, one with lattice contraction by 2% and the other with expansion by 0.4%, were recognized on the La-doped wafer. La Lα fluorescence holograms indicated a complex manner of doping. The simultaneous La cation occupation of the A site, B site, and interstitial site was hypothesized to interpret the atomic images around the fluorescing La cations. This hypothesis needs to be tested further. Composition determined by XPS revealed enrichment of the doping elements, Sr or La, on the wafer surface. Nanometer-scale topography determined by AFM suggested that doping concentrations should be optimized to provide flat, crystalline surfaces suitable for future studies.

ASSOCIATED CONTENT

Supporting Information

The Supporting Information is available free of charge on the ACS Publications website.

Survey-scanned XP spectra of the wafers (PDF)

AUTHOR INFORMATION

Corresponding Author

Hiroshi Onishi, Department of Chemistry, School of Science, Kobe University, Rokko-dai, Nada, Kobe, 657-8501 Japan; Division of Advanced Molecular Science, Institute for Molecular Science, Okazaki, 444-8585 Japan; Email: oni@kobe-u.ac.jp

Authors

Akira Sasahara, Department of Chemistry, School of Science, Kobe University, Rokko-dai, Nada, Kobe, 657-8501 Japan

Koji Kimura, Department of Physical Science and Engineering, Nagoya Institute of Technology, Gokiso, Showa, Nagoya, 466-8555 Japan

Hanggara Sudrajat, Department of Chemistry, School of Science, Kobe University, Rokko-dai, Nada, Kobe, 657-8501 Japan; Research Center for Quantum Physics, The National Research and Innovation Agency, Kawasan Puspitek, Tangerang Selatan 15314 Indonesia

Naohisa Happo, Graduate School of Information Sciences, Hiroshima City University, Hiroshima, 731-3194 Japan

Kouichi Hayashi, Department of Physical Science and Engineering, Nagoya Institute of Technology, Gokiso, Showa, Nagoya, 466-8555 Japan; Japan Synchrotron Radiation Research Institute, SPring-8, Kouto, Sayo, 679-5198, Japan

Author Contributions

The manuscript was written through contributions of all authors.

Notes

The authors declare no competing financial interest.

ACKNOWLEDGMENT

The authors thank Dr. Hirokazu Isumi (Hyogo Prefectural Institute of Technology) for his support in XRD measurements and Dr. Yi Hao Chew (Kobe University) for commenting on the manuscript. X-ray fluorescence holograms were recorded on the BL13XU at SPring-8 through the approval of the Japan Synchrotron Radiation Research Institute (proposal numbers 2017A1079, 2018A1180, and 2019B1499). The financial support provided by Grants-in-Aid for scientific research from the Japanese Society for the Promotion of Science KAKENHI (grant numbers 16H02250, 18F18029, 18KK0161, 19H00915, 21H05547, and 22H00344) is acknowledged. KK, NH, and KH acknowledge the Japanese Society for the Promotion of Science Grants-in-Aid for Transformative Research Areas (A) "Hyper-Ordered Structures Sciences" via grant numbers 20H05878 and 20H05881.

REFERENCES

(1) Wang, Q.; Domen, K. Particulate Photocatalysts for Light-Driven Water Splitting: Mechanisms, Challenges, and Design Strategies. *Chem. Rev.* **2020**, *120*, 919–985.

(2) Inoue, H.; Shimada, T.; Kou, Y.; Nabetani, Y.; Masui, D.; Takagi, S.; Tachibana, H. The water oxidation bottleneck in artificial photosynthesis: how can we get through it? an alternative route involving a two-electron process. *ChemSusChem* **2011**, *4*, 173–179.

(3) Kato, H.; Asakura, K.; Kudo, A. Highly Efficient Water Splitting into H_2 and O_2 over Lanthanum-Doped $NaTaO_3$ Photocatalysts with High Crystallinity and Surface Nanostructure. *J. Am. Chem. Soc.* **2003**, *125*, 3082–3089.

(4) Iwase, A.; Kato, H.; Kudo, A. Nanosized Au Particles as an Efficient Cocatalyst for Photocatalytic Overall Water Splitting. *Catal. Lett.* **2006**, *108*, 7–10.

(5) Sudrajat, H.; Dhakal, D.; Kitta, M.; Sasaki, T.; Ozawa, A.; Babel, S.; Yoshida, T.; Ichikuni, N.; Onishi, H. Electron Population and Water Splitting Activity Controlled by Strontium Cations Doped in $KTaO_3$ Photocatalysts. *J. Phys. Chem. C* **2019**, *123*, 18387–18397.

(6) Sakata, Y.; Hayashi, T.; Yasunaga, R.; Yanaga, N.; Imamura, H. Remarkably high apparent quantum yield of the overall photocatalytic H_2O splitting achieved by utilizing Zn ion added Ga_2O_3 prepared using dilute $CaCl_2$ solution. *Chem. Commun.* **2015**, *51*, 12935–12938.

(7) Takata, T.; Jiang J.; Sakata, Y.; Nakabayashi, M.; Shibata, N.; Nandal, V.; Seki, K.; Hisatomi, T.; Domen, K. Photocatalytic water splitting with a quantum efficiency of almost unity. *Nature* **2020**, *581*, 411–414.

(8) Fujiwara, T.; An, L.; Park, Y.; Happo, N.; Hayashi, K.; Onishi, H. Heteroepitaxial Barium-Doped $NaTaO_3$ Films on $SrTiO_3$(001) Substrate. *Thin Solid Films* **2018**, *658*, 66–72.

(9) Fujiwara, T.; Sasahara, A.; Happo, N.; Kimura, K.; Hayashi, K.; Onishi, H. Single-Crystal Model of Highly Efficient Water-Splitting Photocatalysts: A $KTaO_3$ Wafer Doped with Calcium Cations, *Chem. Mater.* **2020**, *32*, 1439−1447.

(10) Hayashi, K.; Korecki, P. X-Ray Fluorescence Holography: Principles, Apparatus, and Applications. *J. Phys. Soc. Jpn.* **2018**, *87*, 061003.

(11) Vousden, P. A. Study of the Unit-Cell Dimensions and Symmetry of Certain Ferroelectric Compounds of Niobium and Tantalum at Room Temperature. *Acta Cryst.* **1951**, *4*, 373–376.

(12) Liu, X.; Lv, J.; Wang, S.; Li, X.; Lang, J.; Su, Y.; Chai, Z.; Wang, X. A novel contractive effect of $KTaO_3$ nanocrystals via La^{3+} doping and an enhanced photocatalytic performance. *J. Alloys Compd*. **2015**, *622*, 894–901.

(13) Sudrajat, H.; Thushari, I.; Babel, S.; Chemical state and coordination structure of La cations doped in $KTaO_3$ photocatalysts. *J. Phys. Chem. Solids* **2019**, *127*, 94–100.

(14) Ishihara, T.; Nishiguchi, H.; Fukamachi, K.; Takita, Y. Effects of Acceptor Doping to $KTaO_3$ on Photocatalytic Decomposition of Pure H_2O. *J. Phys. Chem. B* **1999**, *103*, 1–3.

(15) Krukowska, A.; Trykowski, G.; Lisowski, W.; Klimczuk, T.; Winiarski, M. J.; Zaleska-Medynska, A. Monometallic nanoparticles decorated and rare earth ions doped $KTaO_3/K_2Ta_2O_6$ photocatalysts with enhanced pollutant decomposition and improved H_2 generation. *J. Catal.* **2018**, *364*, 371–381.

(16) Chen, Z.; Chen, P.; Xing, P.; Hu, X.; Lin, H.; Wu, Y.; Zhao, L.; He, Y. Novel carbon modified $KTa_{0.75}Nb_{0.25}O_3$ nanocubes with excellent efficiency in photocatalytic H_2 evolution. *Fuel* **2018**, *233*, 486–496.

(17) Boddy, P. J.; Kahng, D.; Chen, Y. S. Oxygen Evolution on Potassium Tantalate Anodes. *Electrochimica Acta* **1968**, *13*, 1311–1328.

(18) Paulauskas, I. E.; Katz, J. E.; Jellison, Jr., G. E.; Lewis, N. S.; Boatner, L. A.; Brown, G. M. Growth, Characterization, and Electrochemical Properties of Doped n-type $KTaO_3$ Photoanodes. *J. Electrochem. Soc.* **2009**, *156*, B580–B587.

(19) Ellis, A. B.; Kaiser, W.; Wrighton, M. S. Semiconducor Potassium Tantalate Electrodes. Photoassistance Agents for the Efficient Electrolysis of Water. *J. Phys. Chem.* **1976**, *80*, 1325–1328.

(20) Happo, N.; Hada, T.; Kubota, A.; Ebisu, Y.; Hosokawa, S.; Kimura, K.; Tajiri, H., Matsushita, T.; Hayashi, K. Improvement of Graphite Crystal Analayzer for Light Elements on X-ray Fluorescence Holography Measurement. *Jpn. J. Appl. Phys.* **2018**, *57*, 058006.

(21) Barton, J. J. Removing Multiple Scattering and Twin Images from Holographic Images. *Phys. Rev. Lett.* **1991**, *67*, 3106–3109.

(22) Matsushita, T.; Matsui, F.; Daimon, H.; Hayashi, K. Photoelectron holography with improved image reconstruction, *J. Electron. Spectrosc. Relat. Phenom.* **2010**, *178–179*, 195–220.

(23) Happo, N.; Hayashi, K.; Hosokawa, S. Data Analysis of X-ray Fluorescence Holography by Subtracting Normal Component from Inverse Hologram. *Jpn. J. Appl. Phys.* **2010**, *49*, 116601.

(24) Ebisu, Y.; Hayashi, K.; Happo, N.; Hosokawa, S.; Ozaki, T. Local Structure Analysis of Lanthanum-Doped Strontium Titanate by Means of X-Ray Fluorescence Holography. *Trans. Mat. Res. Soc. Jpn.* **2015**, *40*, 355–358.

(25) Kimura, K.; Urushihara, D.; Kondo, R.; Yamamoto, Y.; Ang, A. K. R.; Asaka, T.; Happo, N.; Hagihara, T.; Matsushita, T.; Tajiri, H.; et al. K. Element-selective local structural analysis around B-site cations in multiferroic $Pb(Fe_{1/2}Nb_{1/2})O_3$ using x-ray fluorescence holography. *Phys. Rev. B* **2021**, *104*, 144101.

(26) Yamamoto, Y.; Kawamura, K.; Sugimoto, H.; Gadelmawla, A.; Kimura, K.; Happo, N.; Tajiri, H.; Webber, K. G.; Kakimoto, K.; Hayashi, K. Significant displacement of calcium and barium ions in ferroelectric $(Ba_{0.9}Ca_{0.1})TiO_3$ revealed by x-ray fluorescence holography. *Appl. Phys. Lett.* **2022**, *120*, 052905.

(27) An, L.; Sasaki, T.; Weidler, P.; Wöll, C.; Ichikuni, N.; Onishi, H. Local Environment of Strontium Cations Activating $NaTaO_3$ Photocatalysts. *ACS Catal.* **2018**, *8*, 880–885.

(28) Konno, R.; Maruyama, S.; Kosaka, T.; Katoh, R.; Takahashi, R.; Kumigashira, H.; Ichikuni, N.; Onishi, H.; Matsumoto, Y. Artificially Designed Compositionally-Graded Sr-Doped $NaTaO_3$ Single-Crystalline Thin Films and the Dynamics of Their Photoexcited Electron-Hole Pairs. *Chem. Mater.* **2021**, *33*, 226–233.

(29) Sudrajat, H.; Kitta, M.; Ito, R.; Nagai, S.; Yoshida, T.; Katoh, R.; Ohtani, B.; Ichikuni, N.; Onishi, H. Water Splitting Activity of La-Doped $NaTaO_3$ Photocatalysts Sensitive to Spatial Distribution of Dopants. *J. Phys. Chem. C* **2020**, *124*, 15285–15294.

(30) Shimura, K.; Kato, S.; Yoshida, T.; Itoh, H.; Hattori, T.; Yoshida, H. Photocatalytic steam reforming of methane over sodium tantalate. *J. Phys. Chem. C* **2010**, *114*, 3493–3503.

(31) Nilsen, W. G.; Skinner, J. G. Raman spectrum of potassium tantalate. *J. Chem. Phys.* **1967**, *47*, 1413–1418.

(32) Smolensky, G. A.; Siny, I. G.; Pisarev, R. V.; Kuzminov, E. G. Raman scattering in ordered and disordered provskite type crystals. *Ferroelectrics* **1976**, *12*, 135−136.

(33) Siny, I. G.; Tao, R.; Katiyar, R. S.; Guo, R.; Bhalla, A. S. J. Raman spectroscopy of Mg–Ta order–disorder in $BaMg_{1/3}Ta_{2/3}O_3$. *Phys. Chem. Solids* **1998**, *59*, 181−195.

(34) An, L.; Onishi, H. Electron−Hole Recombination Controlled by Metal Doping Sites in $NaTaO_3$ Photocatalysts, *ACS Catal.* **2015**, *5*, 3196−3206.

(35) Setvin, M.; Reticcioli, M.; Poelzleitner, F.; Hulva, J.; Schmid, M.; Boatner, L. A.; Franchini, C.; Diebold, U. Polarity compensation mechanisms on the perovskite surface $KTaO_3$(001). *Science* **2018**, *359*, 572–575.

(36) McGuire, G. E.; Schweitzer, G. K.; Carlson, T. A. Study of Core Electron Binding Energies in Some Group IIIa, Vb, and VIb Compounds. *Inorg. Chem.* **1973**, *12*, 2450–2453.

(37) Ghaffari, M.; Shannon, M.; Hui, H.; Tan, O. K.; Irannejad, A. Preparation, surface state and band structure studies of $SrTi_{(1-x)}Fe_{(x)}O_{(3-\delta)}$ (x=0–1) perovskite-type nano structure by X-ray and ultraviolet photoelectron spectroscopy. *Surf. Sci.* **2012**, *606*, 670–677.

(38) van der Heide, P.A.W.; Jiang, Q. D.; Kim, Y. S.; Rabalais, J. W. X-ray photoelectron spectroscopic and ion scattering study of the $SrTiO_3$(001) surface. *Surf. Sci.* **2001**, *473*, 59–70.

(39) De Asha, A. M.; Nix, R. M. Oxidation of lanthanum overlayers on Cu(111). *Surf. Sci.* **1995**, *322*, 41–50.

(40) Uwamino, Y.; Ishizuka, T.; Yamatera, H. X-ray photoelectron spectroscopy of rare-earth compounds. *J. Electron Spectrosc. Relat. Phenom.* **1984**, *34*, 67–78.

(41) Tang, Z.-K.; Di Valentin, C.; Zhao, X.; Liu, L.-M.; Selloni, A. Understanding the Influence of Cation Doping on the Surface Chemistry of $NaTaO_3$ from First Principles. *ACS Catal.* **2019**, *9*, 10528–10535.

(42) Peroviskites, structure-property relationships; R. Tilley; Wiley: New Jersey, 2016. p.10

(43) Yoshioka, K.; Petrykin, V.; Kakihana, M.; Kato, H., Kudo, A. The relationship between photocatalytic activity and crystal structure in strontium tantalates. *J. Catal.* **2005**, *232*, 102–107.

(44) Caldes, M. T.; Deniard, P.; Zou, X. D.; Marchand, R.; Diot, N.; Brec, R. Solving modulated structures by X-ray and electron crystallography. *Micron* **2001**, *32*, 497–507.

(45) Shannon, R. D. Revised Effective Ionic Radii and Systematic Studies of Interatomic Distances in Halides and Chalcogenides. *Acta Cryst. A* **1976**, *32*, 751–767.

(46) Higuchi, M.; Aizawa, K.; Yamaya, K.; Kodaira, K. Electrical Properties of $Sr_{1-x}La_xTiO_3$ ($0 \leqq x \leqq 0.10$) Single Crystals Grown by the Floating Zone Method. *J. Solid State Chem.* **1991**, *92,* 573–577.

(47) An, L.; Kitta, M.; Iwase, A.; Kudo, A.; Ichikuni, N.; Onishi, H., Photoexcited Electrons Driven by Doping Concentration Gradient: Flux-Prepared $NaTaO_3$ Photocatalysts Doped with Strontium Cations. *ACS Catal.* **2018**, *8*, 9334–9341.

(48) Kosaka, T.; Teduka, Y.; Ogura, T.; Zhou, Y.; Hisatomi, T.; Nishiyama, H.; Domen, K.; Takahashi, Y.; Onishi, H. Transient Kinetics of O_2 Evolution in Photocatalytic Water-Splitting Reaction. *ACS Catal.* **2020**, *10*, 13159–13164.

(49) Kosaka, T.; Ando, T.; Hisatomi, T.; Nishiyama, H.; Zhou, Y.; Domen, K.; Takahashi, Y.; Onishi, H. Microelectrode-Based Transient Amperometry of O_2 Adsorption and Desorption on a $SrTiO_3$ Photocatalyst Excited under Water. *Phys. Chem. Chem. Phys.* **2021**, *23*, 19386–19393.

Supporting Information

"$KTaO_3$ Wafers Doped with Sr or La Cations for Modeling Water-Splitting Photocatalysts: 3D Atom Imaging around Doping Cations"

Akira Sasahara[1], Koji Kimura[2], Hanggara Sudrajat1[1,3], Naohisa Happo[4], Kouichi Hayashi[2,5], Hiroshi Onishi[1,6*]

[1]Department of Chemistry, School of Science, Kobe University, Rokko-dai, Nada, Kobe, 657-8501 Japan

[2]Department of Physical Science and Engineering, Nagoya Institute of Technology, Gokiso, Showa, Nagoya, 466-8555 Japan

[3]Research Center for Quantum Physics, The National Research and Innovation Agency, Kawasan Puspitek, Tangerang Selatan 15314 Indonesia

[4]Graduate School of Information Sciences, Hiroshima City University, Hiroshima, 731-3194 Japan

[5]Japan Synchrotron Radiation Research Institute, SPring-8, Kouto, Sayo, 679-5198, Japan

[6]Division of Advanced Molecular Science, Institute for Molecular Science, Okazaki, 444-8585 Japan

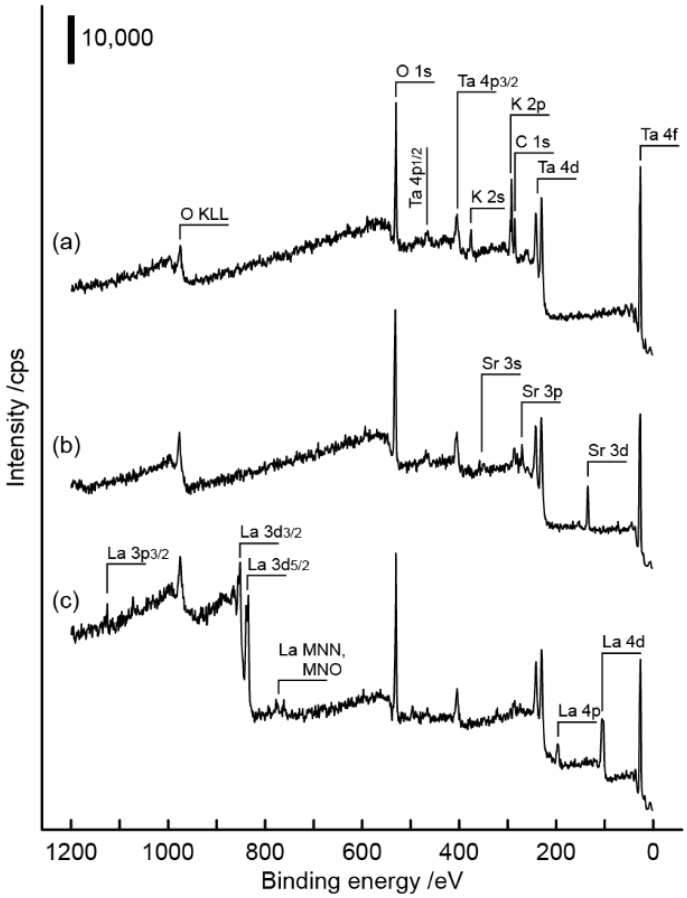

Figure S1. Survey-scanned XPS spectra of (a) as-received, (b) Sr-doped, and (c) La-doped $KTaO_3$(001) wafers. Analyzer pass energy: 280 eV.